Available online at www.sciencedirect.com
ScienceDirect
Journal of the European Ceramic Society 28 (2008) 1227–1234
www.elsevier.com/locate/jeurceramsoc

Preparation and properties of Si_2N_2O/β-cristobalite composites

Qingfeng Tong [a], Jingyang Wang [a], Zhongping Li [b], Yanchun Zhou [a,*]

[a] *Shenyang National Laboratory for Materials Science, Institute of Metal Research, Chinese Academy of Sciences, Shenyang 110016, PR China*
[b] *National Key Laboratory of Advanced Functional Composite Materials, Beijing 100076, PR China*

Received 23 May 2007; received in revised form 17 August 2007; accepted 10 September 2007
Available online 19 November 2007

Abstract

Bulk Si_2N_2O/β-cristobalite composites have been fabricated by a hot-pressing method using Si_3N_4, SiO_2 and Li_2CO_3 as starting materials. β-Cristobalite in the as-sintered composites is successfully stabilized to room temperature through incorporating N and Li into its structure. The introduction of β-cristobalite significantly improves the dielectric properties. Si_2N_2O/62 vol.% β-cristobalite composite shows a low dielectric constant of 4.8 at 1 MHz. In addition, the density, Young's and shear modulus, and strength of the composites decrease with the increase of β-cristobalite content. When the β-cristobalite content is up to 62 vol.%, the flexural strength of the composite reaches 212 MPa. The bulk Si_2N_2O/β-cristobalite composites show the combination of low density, excellent mechanical performance, low dielectric constant and loss tangent, indicating that they are promising high-temperature structural/functional materials.

Keywords: Cristobalite; Mechanical properties; Dielectric properties; SiO_2; Si_2N_2O

1. Introduction

Silicon oxynitride (Si_2N_2O) is a promising structural material for high-temperature applications due to its high strength at high temperatures, excellent oxidation resistance, good thermal shock resistance, low density and high thermal stability (up to 1750 °C).[1,2] However, as a high-temperature functional material, dielectric properties of Si_2N_2O are expected to further improve.[3,4] This can be achieved by introducing other phases with low dielectric constant. Among the high-temperature dielectric materials, including fused SiO_2, BN, Si_3N_4, Al_2O_3 and AlN, fused SiO_2 is preferred because of its very low dielectric constant and loss tangent as well as good thermal shock resistance.[5–8] However, it has some shortcomings, such as low flexural strength and fracture toughness, and the degradation of mechanical properties resulting from softening and crystallization of amorphous SiO_2 above 1100 °C.[8,9]

Compared with fused SiO_2, β-cristobalite possesses an obvious advantage: it can keep its structure stability up to the melting point of SiO_2 (about 1700 °C). In addition, it has good thermal shock resistance and a very low expansion coefficient that even decreases at above 1000 °C.[10–12] Recently, based on ab initio calculations, Xu and Ching[13] predicted that it possesses the lowest dielectric constant in all the crystalline phases of SiO_2. However, β-cristobalite undergoes $\beta \rightarrow \alpha$ displacive phase transition from 170 to 270 °C, depending on the crystallization conditions.[14] This transition is accompanied by 3–5% volume change which often generates great thermal stress and results in the cracking of samples. Thus developing a method to stabilize β-cristobalite to room temperature is of virtual interest.[10–12,15–18]

Adding Al^{3+}, and Na^+, Ca^{2+}, Sr^{2+} or Cu^{2+} by sol–gel route is an effective way to inhibit the phase transition of β-cristobalite. The hindering mechanism was explained as follows: large univalent or divalent cations (Na^+, Ca^{2+}, Sr^{2+} etc.) were stuffed into big interstitial sites of silicate structures to charge-compensate the substitution of Al^{3+} for Si^{4+} in the framework, and the presence of aforementioned cations in the interstices suppressed the contraction of the structure which normally occured during the $\beta \rightarrow \alpha$-cristobalite transition, consequently stabilizing the cubic β-cristobalite structures.[10–12] In addition, the incorporation of $AlPO_4$ could also successfully stabilize the β-cristobalite to room temperature. The mechanism was proposed that the formation of $AlPO_4$-tridymite stacking faults within the β-cristobalite structure interrupted the ⟨1 1 0⟩ chains of corner connecting tetrahedral and inhibited the concerted rota-

* Corresponding author. Tel.: +86 24 23971765; fax: +86 24 23891320.
E-mail address: yczhou@imr.ac.cn (Y. Zhou).

0955-2219/$ – see front matter © 2007 Elsevier Ltd. All rights reserved.
doi:10.1016/j.jeurceramsoc.2007.09.051

tion of these chains, resulting in the preservation of overall β-cristobalite cubic character.[10] However, the materials produced by the aforementioned two methods contained much glassy phase, and a large amount of α-cristobalite formed when the temperature was above 1200 °C.[10–12,15,16] In addition, up to now, bulk β-cristobalite has not been obtained, which prevents further investigation on the properties of β-cristobalite and the application of β-cristobalite as a structural/functional material.

In this paper, bulk Si_2N_2O/β-cristobalite composites were fabricated by a hot-pressing method using Si_3N_4, SiO_2 and Li_2CO_3 as starting materials. β → α-cristobalite displacive phase transition was successfully suppressed. The hindering mechanism was investigated. The mechanical and dielectric properties of Si_2N_2O/β-cristobalite composites were measured. The results obtained in this paper are beneficial to the understanding of properties of β-cristobalite and to the promotion of Si_2N_2O/β-cristobalite composites as candidates for high-temperature structural/functional applications.

2. Experimental procedures

Si_3N_4 powders (average particle size <0.36 μm, oxygen and total metallic impurity contents were 1.5 wt.% and less than 350 ppm, respectively. Sinoma Advanced Materials Co. Ltd., Zhibo, China, SiO_2 powders (99.99% pure, Sinopharm Group Chemical Reagent Co. Ltd., Beijing, China) and Li_2CO_3 powders (99% pure, Sinopharm Group Chemical Reagent Co. Ltd., Beijing, China) were used as starting materials. The molar contents of Si_3N_4, SiO_2 and Li_2CO_3 were modified and listed in Table 1 in order to investigate the influence of Si_3N_4 and Li_2CO_3 on the stabilization of β-cristobalite and to prepare the Si_2N_2O/β-cristobalite composites with various β-cristobalite contents. The mixtures of starting powders were ball-milled in agate jars using Si_3N_4 balls with ethanol medium for 10 h. After being dried and sieved, the powders were put into a high-strength graphite die whose inner surface was pre-sprayed with a layer of BN and then cold-pressed at 5 MPa. Thereafter, the green body together with the die was heated in a nitrogen atmosphere at a heating rate of 10 °C/min to 1550 °C and hot pressed under 30 MPa for 1 h.

The X-ray diffraction (XRD) data of sintered bodies were collected using a step-scanning diffractometer with Cu Kα radiation (Rigaku D/max-2400, Tokyo, Japan). Prior to measurement, the sintered samples were milled and ground with an agar mortar and pestle to obtain fine powders with the particle size of less than 20 μm. The scanning 2θ angle covered a range between 10° and 60° with a step size of 0.02° and a step counting of 5 s. The measurement of all samples was taken under the same conditions. The quantitative phase analyses were performed using the Rietveld method employing the DBWS code in the Cerius[2] computational program for materials research (Molecular Simulation Inc., San Diego, USA).[19]

X-ray photoelectron spectroscopy (XPS) characterization was performed using a X-ray photoelectron spectrometer (ESCALAB 250, Thermo VG, Massachusetts, USA) with Al Kα (1486.6 eV) X-ray resource. The measured binding energies were normalized by the peak energy of C 1s (284.6 eV).

Table 1
The reflection ($h\,k\,l$), 2θ and relative intensity of diffraction peaks associated with cristobalite in Fig. 1a

Samples	Reflection ($h\,k\,l$)	2θ (°)	$I_\alpha/I_{\alpha(1\,0\,1)}$ (%) or $I_\beta/I_{\beta(1\,1\,1)}$ (%)
I			
α-Cristobalite	101	22.00	100.0
	110	25.32	0.6
	111	28.46	7.8
	102	31.48	8.9
	200	36.12	12.6
	112	36.42	3.8
II			
α-Cristobalite	101	22.00	100.0
	110	25.32	0.6
	111	28.46	8.1
	102	31.48	9.1
	200	36.12	14.3
	112	36.42	4.2
III			
Cristobalite		21.80	100.0
		28.24	4.3
		31.20	4.5
		35.88	11.4
IV			
β-Cristobalite	111	21.72	100.0
	220	35.76	13.0
V			
β-Cristobalite	111	21.72	100.0
	220	35.76	12.7

The thermal expansion coefficients of as-sintered samples were determined with a dilatometer (DIL 402, selb, Germany) under a nitrogen flow at a heating rate of 2 °C/min.

The density of as-prepared samples was measured by the Archimedes method. Three-point flexural strength was determined using rectangular bars (3 mm × 4 mm × 40 mm) in a universal testing machine at a crosshead speed of 0.5 mm/min. Fracture toughness (K_{IC}) was determined by an indentation technique with a load of 49 N and a dwell time of 15 s. The fracture toughness was calculated using the equation proposed by Anstis et al.[20]

The Young's modulus and shear modulus at room temperature were evaluated in a RFDA-HTVP1750-C testing machine (IMCE, Diepenbeek, Belgium). The samples were rectangular bars of 3 mm × 15 mm × 40 mm in size. The Young's modulus and shear modulus were calculated according to the ASTM standard E 1259-94.

The dielectric constant and loss tangent were determined using 4294A Impedance Analyzer and 16451B Dielectric Test Fixture (Agilent, California, USA). The frequency ranged from 40 Hz to 20 MHz. The microstructures of bulk samples were observed in a SUPRA 35 scanning electron microscope (LEO, Oberkochen, Germany). Before SEM observation, the samples were etched in a 1:1 HF/HNO_3 solution for 5 min.

3. Results and discussion

3.1. Stabilization of β-cristobalite

Amorphous SiO_2 without dopant and amorphous SiO_2 doped with 2 mol% Li_2CO_3 and different amounts of Si_3N_4 were sintered at 1550 °C for 1 h. XRD patterns of the as-prepared samples are presented in Fig. 1a. The magnifications of the corresponding reflections in Fig. 1a in the range of $2\theta = 17–37°$ are presented in Fig. 1b–e, to identify crystal structure characteristic of cristobalite. The relative intensities and 2θ of peaks in Fig. 1a associated with cristobalite are listed in Table 1. For SiO_2 without dopant and doped with only 2 mol% Li_2CO_3, α-cristobalite is the only crystalline phase (compositions I and II in Fig. 1a). Its main reflections in the range of $2\theta = 17–37°$ are at 22.00°, 28.46°, 31.48°, 36.12° and 36.42° (composition II in Fig. 1b–e), corresponding to (1 0 1), (1 1 1), (1 0 2), (2 0 0) and (1 1 2), respectively. Their relative intensities are 100:8:9:13:4. When 6 mol% Si_3N_4 is added, the $(1\,1\,2)_\alpha$ reflection disappears (composition III in Fig. 1e) and the other four reflections associated with cristobalite in the range of $2\theta = 17–37°$ shift toward lower angles ($2\theta = 21.80°$, 28.24°, 31.20° and 35.88°) and their relative intensities change to 100:4:5:11 (composition III in Fig. 1a–e), indicating that N is incorporated into the structure of α-cristobalite and causes the increase of lattice spacing. When 16 mol% Si_3N_4 is doped, the two characteristic peaks of α-cristobalite ($2\theta = 28.24°$ and 31.20°) disappear (composition IV in Fig. 1c and d) and the other two peaks

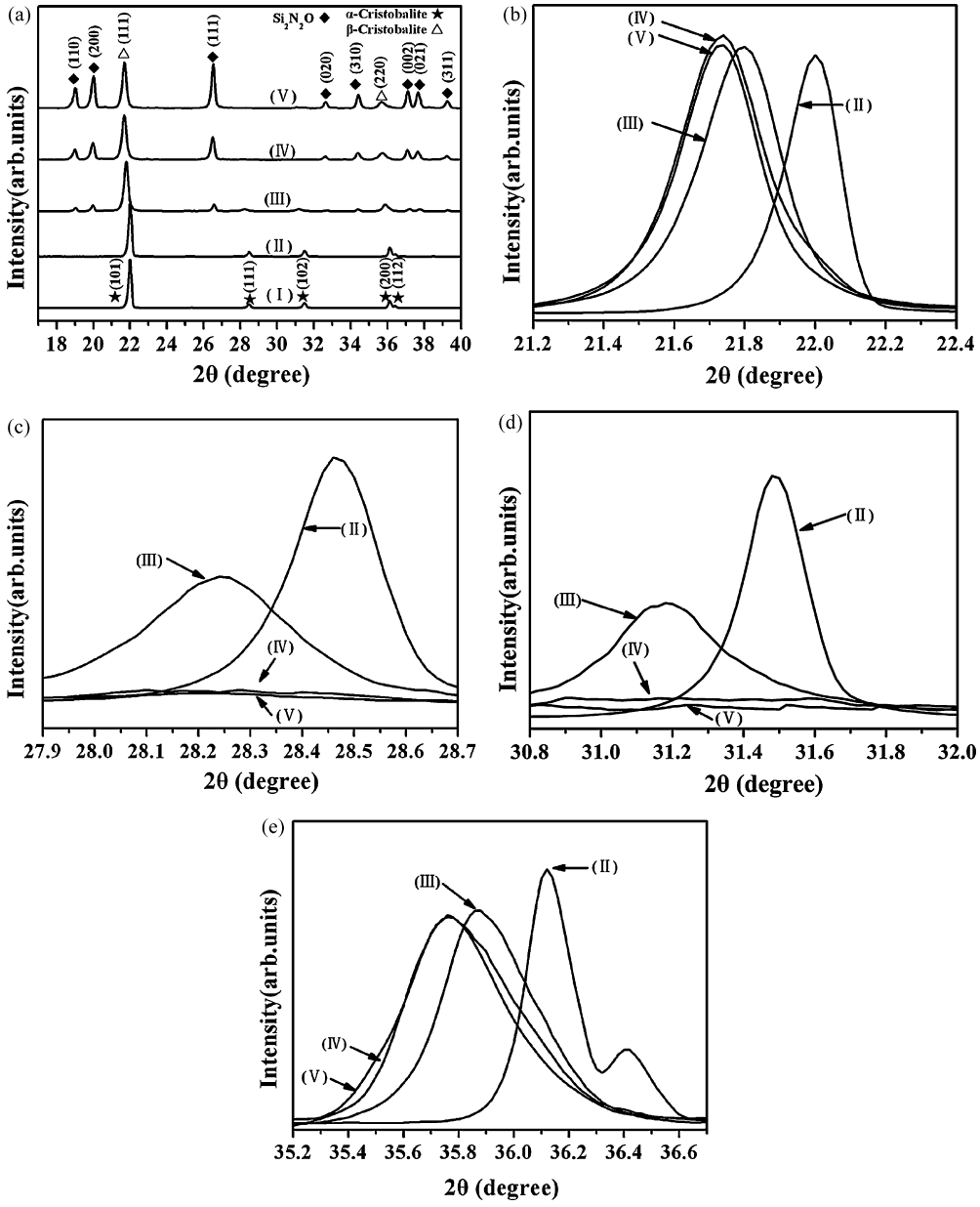

Fig. 1. X-ray diffraction patterns of as-sintered samples with different initial materials: (I) SiO_2, (II) SiO_2 + 2 mol% Li_2CO_3, (III) SiO_2 + 2 mol% Li_2CO_3 + 6 mol% Si_3N_4, (IV) SiO_2 + 2 mol% Li_2CO_3 + 16 mol% Si_3N_4, (V) SiO_2 + 2 mol% Li_2CO_3 + 25 mol% Si_3N_4. (b)–(e) are the magnifications of corresponding reflections in $2\theta = 21.2–22.4$, 27.9–28.7, 30.8–32.0 and 35.2–36.8, respectively.

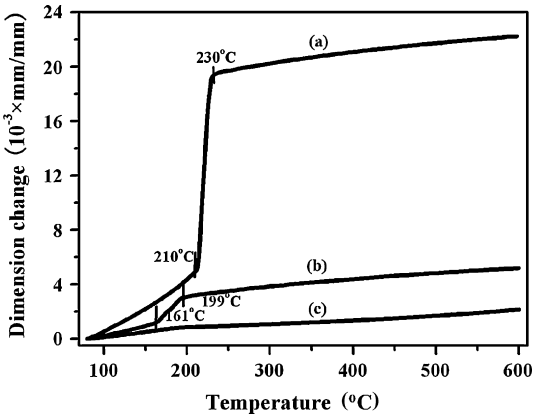

Fig. 2. Thermal expansion of as-sintered samples doped with 2 mol% Li_2CO_3 and different amounts of Si_3N_4: (a) 0 mol% Si_3N_4, (b) 6 mol% Si_3N_4 and (c) 16 mol% Si_3N_4.

shift to $2\theta = 21.72°$ and 35.76° (composition IV in Fig. 1b and e), respectively, which correspond to (1 1 1) and (2 2 0) of β-cristobalite. This demonstrates that the introduction of 16 mol% Si_3N_4 can lead to the stabilization of the high temperature phase, β-cristobalite, to room temperature. Further increasing the Si_3N_4 content does not change the positions of (1 1 1) and (2 2 0) peaks (composition V in Fig. 1b and e). The stabilization of β-cristobalite in the as-sintered sample doped with 16 mol% Si_3N_4 can also be confirmed by its thermal expansion behavior. Its dimension continuously changes with temperature (Fig. 2c). Whereas the unstabilized cristobalite, obtained by sintering SiO_2 with 2 mol% Li_2CO_3, shows large discontinuous volume expansion at 210–230 °C, associated with the characteristic first-order $\alpha \rightarrow \beta$ transition (Fig. 2a). The addition of 6 mol% Si_3N_4 greatly reduces the volume expansion because a part of β-cristobalite is stabilized to room temperature (Fig. 2b).

It can be seen from Fig. 1a (III) that in the presence of 2 mol% Li_2CO_3, doping 16 mol% Si_3N_4 into SiO_2 yields the mixtures of Si_2N_2O and chemically stabilized β-cristobalite at room temperature, indicating that a part of nitrogen in Si_3N_4 reacts with SiO_2 to form Si_2N_2O and the other may dissolve into the structure of β-cristobalite and contribute to its stabilization. Nitrogen atom has a similar radius to oxygen and the Si–N (0.174 nm) and Si–O (0.170 nm) bond lengths are very close, implying the easy substitution of nitrogen for oxygen atom of $SiO_{4/2}$ tetrahedron in cristobalite.[21,22] To compensate charge for the substitution, Li^+ is probably stuffed into the big interstitial sites formed by six-membered rings of $SiO_{4/2}$ tetrahedral in the cristobalite structure. Fig. 3 shows the schematic structure of stabilized β-cristobalite by nitrogen and Li along (1 1 0) direction.

In order to further confirm that nitrogen atoms substitute oxygen atoms in cristobalite structure, X-ray photoelectron spectroscopy (XPS) was used to analyze the as-sintered samples doped with 2 mol% Li_2CO_3 and different amounts of Si_3N_4 (Fig. 4). For the as-prepared sample with 50 mol% Si_3N_4 in starting material, its only crystalline phase is Si_2N_2O (see Fig. 5e). And its N 1s binding energy are 397.7 eV (Fig. 4a), which is in agreement with that measured by Finster et al.[23] When the molar contents of Si_3N_4 in the starting materials are decreased to 16%

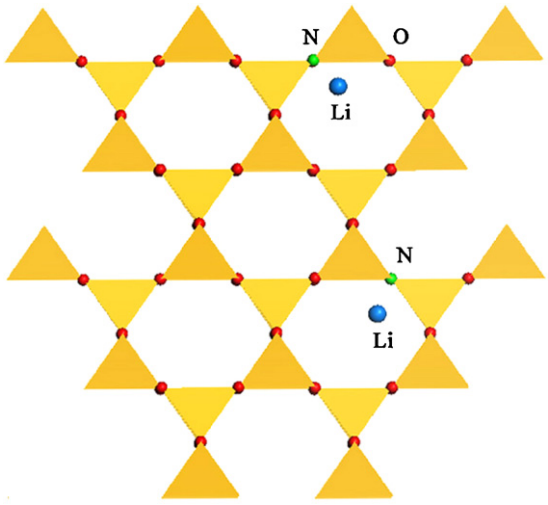

Fig. 3. Schematic polyhedral representation of stabilized β-cristobalite doped with nitrogen and lithium along (1 1 0) direction.

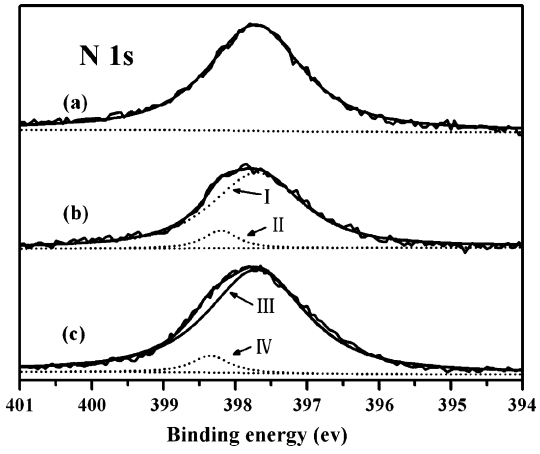

Fig. 4. XPS spectra of N 1s for the as-sintered samples doped with 2 mol% Li_2CO_3 and different amounts of Si_3N_4: (a) 50 mol% Si_3N_4, (b) 16 mol% Si_3N_4 and (c) 6 mol% Si_3N_4.

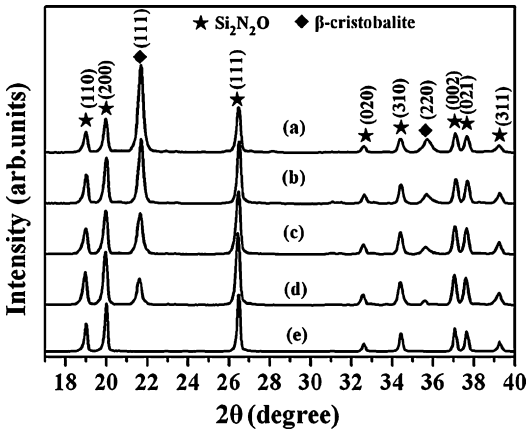

Fig. 5. X-ray diffraction patterns of as-sintered samples with SiO_2 + 2 mol% Li_2CO_3 + different amounts of Si_3N_4 as starting materials: (a) 16 mol% Si_3N_4, (b) 25 mol% Si_3N_4, (c) 30 mol% Si_3N_4, (d) 40 mol% Si_3N_4 and (e) 50 mol% Si_3N_4.

and 6%, the as-sintered samples are composed of Si_2N_2O and cristobalite (III and IV in Fig. 1a). Their N 1s core level spectra are shown in Fig. 4b and c, respectively, and deconvoluted using a Gaussian function. Both peak I in Fig. 4b and peak III in Fig. 4c are centered at 397.7 eV, which are attributed to Si_2N_2O. Peak II in Fig. 4b and peak IV in Fig. 4c show a remarkable difference: their binding energies are 398.2 eV and 398.4 eV, respectively, which are close to that of N1s in oxynitride glasses.[24] The two peaks can be assigned to cristobalite. N1s peak for cristobalite in the sample doped with 16 mol% Si_3N_4 shifts 0.2 eV to the lower binding energy range compared with the sample doped with 6 mol% Si_3N_4. This is due to the fact that more nitrogen atoms are incorporated into the structure of cristobalite with the increase of Si_3N_4, resulting in the change of local charge. The similar phenomenon was found in oxynitride glasses and vapor-deposited oxynitride films: the binding energy of N 1s slightly decreases when more oxygen atoms in oxynitride structure are replaced by nitrogen atoms.[24,25]

3.2. Preparation and microstucture of bulk Si_2N_2O/β-cristobalite composites

SiO_2, 2 mol% Li_2CO_3 and different amounts of Si_3N_4 were used as starting materials and hot-pressed at 1550 °C to prepare bulk Si_2N_2O/stabilized β-cristobalite composites. Fig. 5 shows XRD patterns of the as-sintered samples. It can be seen that the as-prepared samples are well crystallized and only β-cristobalite and Si_2N_2O are identified. No peak for other crystalline phases can be detected via XRD. The intensity ratios of β-cristobalite (1 1 1) to Si_2N_2O (1 1 1) increase with the decrease of Si_3N_4 content. When the Si_3N_4 content in starting materials is less than 16 mol%, much crack is observed in the as-sintered sample because the amount of Si_3N_4 is not sufficient to effectively suppress the phase transition of β → α-cristobalite and high thermal stress is generated. The true contents of β-cristobalite in the as-sintered samples are calculated using the Rietveld method and are shown in Table 2.

The microstructure of Si_2N_2O/β-cristobalite composite with 62 vol.% β-cristobalite is presented in Fig. 6. Si_2N_2O and β-cristobalite have similar contrast and can not be distinguished in SEM. However, it can be seen that grains of the composite exhibit plate-like shape with an average size of 3–5 μm. The similar grain morphology was also found in stabilized β-cristobalite by adding Al_2O_3 and Na_2O.[12,17]

Table 2
The molar ratio of composition in starting materials and the β-cristobalite contents in as-sintered samples calculated by the Rietveld method

The molar ratio of composition in starting materials			The calculated contents of β-cristobalite	
Li_2CO_3	Si_3N_4	SiO_2	vol.%	wt.%
0.02	0.50	0.48	0	0
0.02	0.35	0.63	27	22
0.02	0.25	0.53	44	38
0.02	0.20	0.78	53	47
0.02	0.16	0.82	62	56
0.02	0.06	0.92	–	–
0.02	0	0.98	–	–
0	0	1	–	–

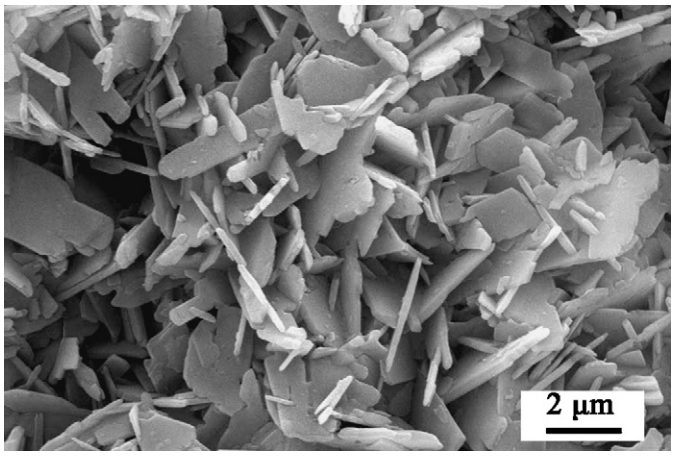

Fig. 6. Scanning electron micrograph of Si_2N_2O/62 mol% β-cristobalite composite. The sample was etched by a 1:1 HF/HNO_3 solution for 5 min.

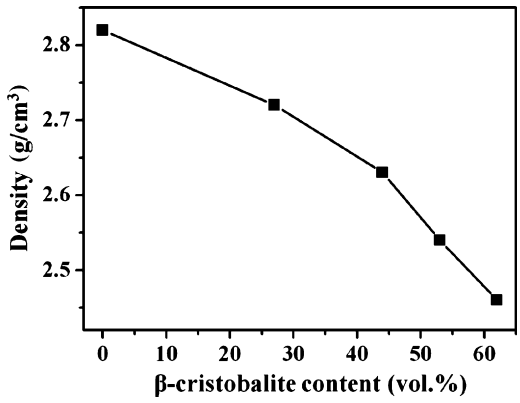

Fig. 7. Density of Si_2N_2O/β-cristobalite composites as a function of β-cristobalite content.

3.3. Mechanical properties of bulk Si_2N_2O/β-cristobalite composites

Figs. 7 and 8 display the density, Youngs' modulus and shear modulus of Si_2N_2O/β-cristobalite composites versus β-

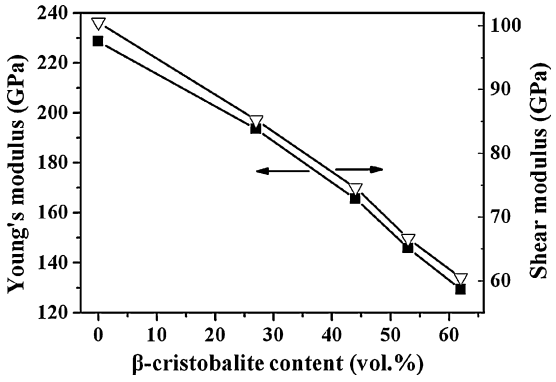

Fig. 8. Young's and shear modulus of Si_2N_2O/β-cristobalite composites as a function of β-cristobalite content.

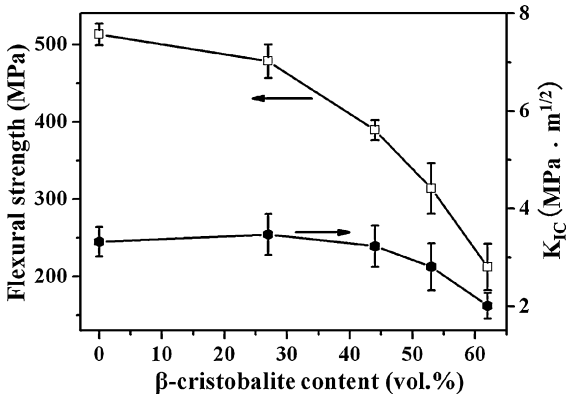

Fig. 9. Flexural strength and fracture toughness of Si_2N_2O/β-cristobalite composites as a function of β-cristobalite content.

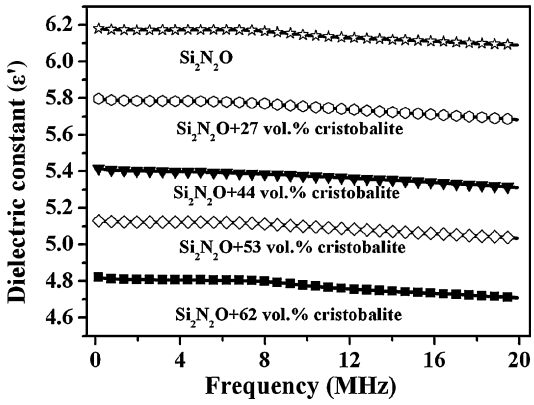

Fig. 10. The frequency dependence of dielectric constant of Si_2N_2O/β-cristobalite composites with various β-cristobalite content.

cristobalite content. These properties decline with the increase of β-cristobalite contents. The density value of Si_2N_2O/62 vol.% β-cristobalite composite is 87% of monolithic Si_2N_2O. Young's modulus decreases by 44% from 228.6 GPa for monolithic Si_2N_2O to 129.3 GPa for Si_2N_2O/62 vol.% β-cristobalite composite. The corresponding decrease in shear modulus is 40% from 100.5 to 60.5 GPa. The elastic properties of β-cristobalite are not available in literature, however, it can be postulated from the properties of Si_2N_2O/β-cristobalite composites that similar to amorphous SiO_2, β-cristobalite possesses low Young's and shear modulus.

Fig. 9 shows the strength and fracture toughness of Si_2N_2O/β-cristobalite composites versus β-cristobalite content. The fracture toughness of the composites is between 2.0 and 3.9. The flexural strength of the composites decreases with the increase of β-cristobalite content. When the content of β-cristobalite is 62 vol.%, the flexural strength of the composite is 212 MPa.

3.4. Dielectric properties of bulk Si_2N_2O/β-cristobalite composites

Besides mechanical properties, dielectric constant is another important parameter of structural/functional material. Dielectric constant ε' and loss tangent tg δ of Si_2N_2O/β-cristobalite composites with various β-cristobalite contents as a function of frequency are determined and are shown in Figs. 10 and 11, respectively. It can be seen that dielectric constant ε' of the composites slightly deceases with the increase of frequency. For ceramics with low dielectric constant, space charge polarization is considered to be the main polarization mechanism and the relaxation time τ is relatively long.[26] Therefore, as the frequency increases, space charge polarization can not follow the changing electromagnetic field, resulting in the decrease of dielectric constant. Si_2N_2O/β-cristobalite composites exhibit the low loss tangent, which is below 0.007 in the frequency range of 40 Hz to 20 MHz.

It can be seen from Fig. 10 that the introduction of β-cristobalite effectively lowers the dielectric constant. The dielectric constants of the composites vesus β-cristobalite content at 1 MHz are plotted in Fig. 12. The dielectric constant decreases from 6.17 for monolithic Si_2N_2O to 4.81 for Si_2N_2O/62 vol.% β-cristobalite composite. The following equation is proposed by Wakino et al.[27] and has been widely used to calculate the dielectric constant of a composite:

$$\varepsilon_r^{\alpha} = V_1\varepsilon_1^{\alpha} + V_2\varepsilon_2^{\alpha} \quad (1)$$

where ε_1^{α}, ε_2^{α} and ε_r^{α} are the dielectric constants of material 1, material 2 and the mixture of material 1 and material 2, respectively, and V_1 and V_2 are the volume fraction of material 1 and material 2, respectively, and α is a constant. The equation is

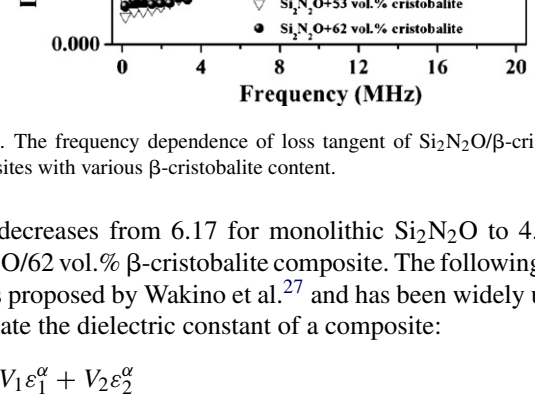

Fig. 11. The frequency dependence of loss tangent of Si_2N_2O/β-cristobalite composites with various β-cristobalite content.

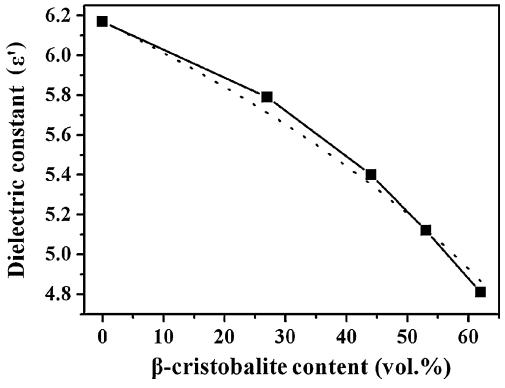

Fig. 12. Dielectric constant of Si_2N_2O/β-cristobalite composites at 1 MHz as a function of β-cristobalite content.

Table 3
Selected properties of several structural/functional ceramics

Properties	Si_2N_2O	Si_3N_4[28,29]	Al_2O_3[28,30]	AlN[28]	Hexagonal BN[28]	Fused SiO_2[5,28]	Si_2N_2O/62 vol.% β-cristobalite
ρ (g/cm^3)	2.81	3.18	3.98	3.2	2.27	2.2	2.46
E (GPa)	289	320	416	330	77.9	72	129
σ_b (MPa)	513	700	380	280	89.6	50	212
K_{IC} (MPa m$^{1/2}$)	3.3	4.5	2.7	2.6	–	1.0	2.0
H_V (GPa)	17	16.5	18	12	2 (Morse)	7	9.1
ε' (1 MHz)	6.2	9	9.9	9.4	4.2	3.9	4.8
tg δ (1 MHz)	0.0008	0.002	0.00023	0.002	0.0002	0.0003	0.0009

used to fit the relationship curve between the β-cristobalite content and dielectric constant of the composites at 1 MHz. The dielectric constant of β-cristobalite at 1 MHz is determined to be 4.07, which is higher than the calculated value by the first-principle method.[13] The measured high dielectric constant may be associated with the increasing polarization resulting from the substitution of O by N and the stuffing of Li^+ into the interstice in β-cristobalite structure.

Table 3 lists the properties of some high-temperature structural/functional materials with low dielectric constant and loss tangent.[5,28–30] Si_2N_2O/62 vol.% β-cristobalite composite exhibits lower dielectric constant than Si_2N_2O, Si_3N_4, Al_2O_3, and AlN. This composite has a density of 2.46 g/cm^3, which is lower than that of Si_2N_2O, Si_3N_4, Al_2O_3 and AlN and is close to that of fused SiO_2 and hexagonal BN. Its flexural strength 212 MPa is about twice higher than that of hot-pressed hexagonal BN and is comparable to that of AlN.

Fused SiO_2 has received much attention as a high temperature functional material due to its excellent dielectric properties and excellent thermal shock resistance.[5–8] However, its application is limited because of unsatisfactory mechanical properties and softening and the crystallization of amorphous SiO_2 above 1100 °C.[8,9] It can be seen from Table 2 that compared with fused SiO_2, Si_2N_2O/62 vol.% β-cristobalite composite possesses slightly inferior dielectric properties, however, its flexural strength and fracture toughness are about four times and twice in excess of those of fused SiO_2, respectively. In addition, Si_2N_2O/62 vol.% β-cristobalite composite can keep chemical stability up to the melting point of β-cristobalite (about 1700 °C), indicating that it is a potential high temperature structural/functional material.

4. Conclusions

1. Bulk Si_2N_2O/β-cristobalite composites with various β-cristobalit contents were synthesized using Si_3N_4, SiO_2 and Li_2CO_3 as starting materials by a hot-pressing method.
2. The β → α-cristobalite first-order transition is effectively hindered in the as-sintered composites doped with more than 16 mol% Si_3N_4 and 2 mol% Li_2CO_3.
3. The density, Young's and shear modulus, flexural strength of the as-sintered composites decrease with increasing β-cristobalite content. When the β-cristobalite content is 62 vol.%, the flexural strength of the composite reaches 212 MPa.
4. The introduction of β-cristobalite remarkably improves the dielectric properties. Si_2N_2O/β-cristobalite composite with 62 vol.% β-cristobalite shows a low dielectric constant of 4.8 at 1 MHz.

Acknowledgements

This work was supported by the National Outstanding Young Scientist Foundation of China under grant nos. 59925208, Natural Sciences Foundation of China under grant nos. 50232040, 50072034, 90403027, 863 project, 973 project and High-tech Bureau of the Chinese Academy of Sciences.

References

1. Ohashi, M., Tabata, H. and Kanzaki, S., High-temperature flexural strength of hot-pressed silicon oxynitride ceramics. *J. Mater. Sci. Lett.*, 1988, **7**(4), 339–340.
2. Ohashi, M., Kanzaki, S. and Tabata, H., Effect of additives on some properties silicon oxynitride ceramics. *J. Mater. Sci.*, 1991, **26**(10), 2608–2614.
3. Tong, Q. F., Wang, J. Y., Li, Z. P. and Zhou, Y. C., Low-temperature synthesis/densification and properties of Si_2N_2O with Li_2O additive. *J. Eur. Ceram. Soc.*, 2007, **27**(16), 4767–4772.
4. Shen, Q., Chen, F., Yan, F. Q. and Zhang, L. M., Progress on new type high temperature ceramic missiles radome materials. *Mater. Rev.*, 2006, **20**(9), 1–4 (in Chinese).
5. Lyons, J. S. and Starr, T. L., Strength and toughness of slip-cast fused-silica composites. *J. Am. Ceram. Soc.*, 1994, **77**(6), 1673–1675.
6. Wen, G., Wu, G. L., Lei, T. Q., Zhou, Y. and Guo, Z. X., Co-enhanced SiO_2-BN ceramics for high-temperature dielectric applications. *J. Eur. Ceram. Soc.*, 2000, **20**(12), 1923–1928.
7. Walton JR, J. D., Reaction sintered silicon nitride for high temperature radome applications. *Ceram. Bull.*, 1974, **53**(3), 255–258.
8. Bruckner, R., Properties and structure of vitreous silica. *J. Non-Cryst. Solids*, 1970, **5**(3), 123–175.
9. Wagstaff, F. E., Crystallization kinetics of internally nucleated vitreous sillica. *J. Am. Ceram. Soc.*, 1968, **51**(8), 449–453.
10. Thomas, E. S., Thompson, J. T. and Withers, R. L., Further investigation of the stabilization of β-cristobalite. *J. Am. Ceram. Soc.*, 1994, **77**(1), 49–56.
11. Saltzberg, M. A., Bors, S. L., Bergna, H. and Winchester, S. C., Synthesis of chemically stabilized cristobalite. *J. Am. Ceram. Soc.*, 1992, **75**(1), 89–95.
12. Perrotta, A. J., Grubbs, D. K., Martin, E. S., Dando, N. R., Mckinstry, H. A. and Huang, C. Y., Chemical stabilization of β-cristobalite. *J. Am. Ceram. Soc.*, 1989, **72**(3), 441–447.
13. Xu, Y. N. and Ching, W. Y., Electronic and optical properties of all polymorphic forms of silicon dioxide. *Phys. Rev. B*, 1991, **44**(20), 11048–11059.
14. Hatch, D. M. and Ghose, S., The α–β phase transition in cristobalite, SiO_2: symmetry analysis, domain structure, and the dynamical nature of the β phase. *Phys. Chem. Miner.*, 1991, **17**(6), 554–562.
15. Perrotta, A. J., Grubbs, D. K. and Martin, E. S., Process for preparing stabilized high cristobalite. U.S. Pat. No. 4818729, April 4, 1989.

16. Alcala, M. A., Real, C. and Criado, J. M., A new "incipient-wetness" method for the synthesis of chemically stabilized β-cristobalite. *J. Am. Ceram. Soc.*, 1996, **79**(6), 1681–1684.
17. Chao, C. H. and Lu, H. Y., Stress-induced β → α-cristobalite phase transformation in ($Na_2O + Al_2O_3$)-codoped silica. *Mater. Sci. Eng. A*, 2002, **328**(1/2), 267–276.
18. Lee, S. J. and Lee, C. H., Critical size effect for chemically doped β-cristobalite transformation. *Mater. Lett.*, 2000, **45**(3–4), 175–179.
19. Young, R. A., *The Rietveld Method*. Oxford University Press, 1993.
20. Anstis, G. R., Chantikul, P., Lawn, B. R. and Marshall, D. B., A critical evaluation of indentation techniques for measuring fracture toughness. I. Direct crack measurements. *J. Am. Ceram. Soc.*, 1981, **64**(9), 533–538.
21. Loehman, R. E., Oxynitride glasses. *J. Non-Cryst. Solids*, 1980, **42**(1–3), 433–446.
22. Hampshire, S., Oxynitride glasses, their properties and crystallisation—a review. *J. Non-Cryst. Solids*, 2003, **316**(1), 64–73.
23. Finster, J., Klinkenberg, E. D. and Heeg, J., ESCA and SEXAFS investigations of insulating materials for ULSI microelectronics. *Vacuum*, 1990, **41**(7–9), 1586–1589.
24. Brow, R. K. and Pantano, C. G., Nitrogen coordination in oxynitride glasses. *J. Am. Ceram. Soc.*, 1984, **67**(4), C72–C74.
25. Raider, S. I., Flitsch, R., Aboaf, J. A. and Pliskin, W. A., Surface oxidation of silicon nitride films. *J. Electrochem. Soc.*, 1976, **123**(3), 560–565.
26. Cai, K. F. and Mclachlan, D. S., Preparation, microstructure, and properties of reaction-bonded AlN ceramics. *Mater. Res. Bull.*, 2002, **37**(3), 575–581.
27. Wakino, K., Okada, T., Yoshida, N. and Tomono, K., A new equation for predicting the dielectric constant of a mixture. *J. Am. Ceram. Soc.*, 1993, **76**(10), 2588–2594.
28. Ceramic properties databases of the American Ceramic Society. Available from: http://www.matweb.com/search/SpecificMaterial.aspbassnum.
29. Hampshire, S., Engineering properties of nitrides. In *Engineered Materials Handbook*, *Vol 4*, ed. S. J. Schneider Jr. ASM International, 1991, pp. 812–820.
30. Munro, R. G., Evaluated material properties for a sintered alpha-Al_2O_3. *J. Am. Ceram. Soc.*, 1997, **80**(8), 1919–1928.